Flexural failure modes of ribbed triangular UHPFRC plates: experimental and numerical investigation

Thomas Guénet [1,2], Florent Baby [1], Pierre Marchand [1], Luca Sorelli [2], Sébastien Bernardi [3], François Toutlemonde [1]

[1] Paris-Est University-IFSTTAR, Materials and Structures Department, Marne-la-Vallée, France
[2] Laval University, Civil Engineering Department, Québec, Canada
[3] LafargeHolcim, Ductal® Technical Direction, Paris, France

Abstract:

Thin UHPFRC plates stiffened by reinforced ribs represent a promising use of UHPFRC as demonstrated in some outstanding applications. Optimization of the ribs reinforcement and of the UHPFRC fibre ratio, which has significant economic and technical relevance, is critically related to guaranteeing ductile failure modes of such structures and components, including effects of the scatter of local material properties and post-cracking fibre contribution. A micromechanical model based on the fibre pull-out mechanism and explicitly accounting for fibre orientation and spatial dispersion has been developed and its ability to support the structural design of ribbed reinforced UHPFRC structures is under validation. To this aim, flexural tests on ribbed triangular UHPFRC plates have been carried out at IFSTTAR Structures Laboratory, with LafargeHolcim as a partner, in a joint project with Laval University. The fibre content and the preferential fibre orientation related to casting process were varied, as well as the loading configuration, so that the possible structural redundancy could be checked. The results of these tests are described and numerically analysed in relation to the material properties derived from both molded samples and specimens sawn from companion plates.

Keywords: UHPFRC, UHPC, steel fibres, ribbed plates, fibre orientation, micromechanics.

1. Introduction

Ultra High Performance Fibre-Reinforced Concrete (UHPFRC) refers to a class of fiber reinforced cement-based materials with a characteristic compressive strength in excess of 130 MPa, and containing steel fibres in order to achieve ductile behaviour under tension (NF P18-470, 2016). Indeed the UHPFRC tensile behaviour is a fundamental constitutive property which affects the use of the conventional reinforcement. UHPFRC technology allows designing lightweight and durable elements, which can be also prestressed for achieving longer span. Moreover, UHPFRC plates stiffened by reinforced ribs represent a conceptual efficient use of UHPFRC, as demonstrated in some previous applications, e.g., Villa Navarra roofing, Jean Bouin arena renovation (Ricciotti *et al.*, 2011 ; Mazzacane *et al.*, 2013), etc.. However, the flexural behavior of UHPFRC plates under bidirectional loading has not been extensively documented for UHPFRC. Besides the optimization of the ribs reinforcement and of the UHPFRC fibre ratio, which has significant economic and technical relevance, is critical to guarantee the ductile failure modes of such structures and components, especially considering the effect of the scatter of fiber distribution on the local post-cracking behavior. Therefore, the

design of ribbed UHPFRC plates needs to be still optimized by developing reliable Finite Element Method (FEM) models which consider the fibre orientation and dispersion.
In this work, we employed a new fracture micro-mechanics model which has been lately developed to statistically describe the effect of the fiber orientation distribution on the local post-cracking behavior as detailed in (Sorelli *et al.*, 2007 ; Guénet *et al.*, 2013). In particular, the fiber orientation distribution is represented by a bi-variate normal-like probability density function.The ability of the model to support the structural design of ribbed reinforced UHPFRC structures is under validation. Therefore an experimental program was defined to analyse the flexural behaviour of reinforced ribbed triangular UHPFRC plates taking into account the actual orientation of fibres. The model is calibrated on results from UHPFRC mechanical characterization derived from both molded samples and specimens sawn from companion plates. Then, the FEM implementation of the micromechanics model is applied to study the flexural tests of the reinforced ribbed triangular UHPFRC plates.

2. Flexural tests

2.1. Specimens and parameters

All specimens were fabricated in a precast factory (Bonna Sabla, Vendargues, France), using UHPFRC mixes with two fiber ratios (V_f = 1% and V_f = 2%), with main features presented in Table 1. At 48 hours, the specimens were heat treated for 48 hours in a climate-conditioned box at about 90°C with a relative humidity of about 100 %. Such heat treatment allows rapidly increase the mechanical properties and to complete maturation of the UHPFRC mix. As a consequence, after the heat treatment, no further shrinkage occurs and the creep is significantly reduced. The main parameters studied in this experimental program were: (i) the fiber ratio; (ii) the casting process; and (iii) the loading configuration. Ten UHPFRC plates stiffened by reinforced ribs were tested. An overview of specimens characteristics is given in Table 2.

Table 1. UHPFRC mix characteristics

Concrete Mix	**f_c cylinders (110mm*220mm) After steam treatment (MPa)**	**Young's Modulus After steam treatment (GPa)**	**Steel straight fibers $L_f - \Phi_f$ (mm)**	**V_f (%)**
UHPFRC-1%	229	56.9	13 – 0.2	1.0
UHPFRC-2%	234	58.4	13 – 0.2	2.0

The triangular specimens got a total length of 2.25 meters having a span of 2.0 meters and a total depth of 160 mm. Each rib was reinforced thanks to #16 rebar with an effective depth equal to 130 mm. The ribs width was 60 mm. The nominal top flange thickness was 35 mm for all specimens, however 1 or 2 mm-deviation was observed and taken into account in the results interpretation. The full details of dimensions and arrangement of reinforcement are shown in Figure 1.
Two casting processes have been considered in order to estimate their influence on fiber orientation in the structure: casting process A or B. The process A aims to obtaining an isotropic fiber orientation in the deck plane. The process B corresponds to a casting method trying to induce preferential fibre orientation (in the deck plane) following the transverse direction.
Two loading configurations have been considered (see Figure 2). The first configuration is a Four Point Bending Test (4BPT) chosen to grasp the behavior of reinforced UHPFRC and

quantify the possible contribution of the deck in-between the ribs. The position of four loading points has been determined in order to obtain a quasi-constant stress on the tensile face in-between. The second configuration is a centred bending test which aims to grasp the UHPFRC behavior under complex loading (concomitance of longitudinal and transversal bending) with identification of forces redistribution after structural localization and yield lines pattern.

Table 2. Parameters of the flexural tests

Specimen	Fiber ratio	Casting process	Loading configuration
2%-A-4pts-01	2%	Process A	4 point bending
2%-A-4pts-02	2%	Process A	4 point bending
1%-B-4pts-01	1%	Process B	4 point bending
1%-B-4pts-02	1%	Process B	4 point bending
2%-A-centred-01	2%	Process A	Centred bending
2%-A-centred-02	2%	Process A	Centred bending
1%-A-centred-01	1%	Process A	Centred bending
1%-A-centred-02	1%	Process A	Centred bending
1%-B-centred-01	1%	Process B	Centred bending
1%-B-centred-02	1%	Process B	Centred bending

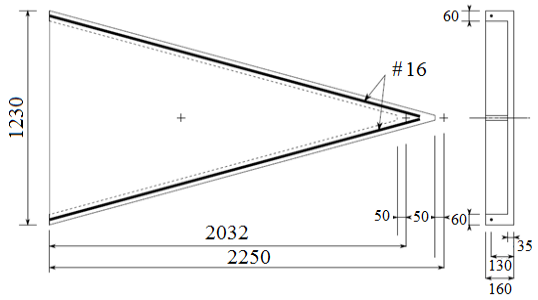

Figure 1. Top view of specimens (Left side) and cross-section (Right side) – Dimensions in mm

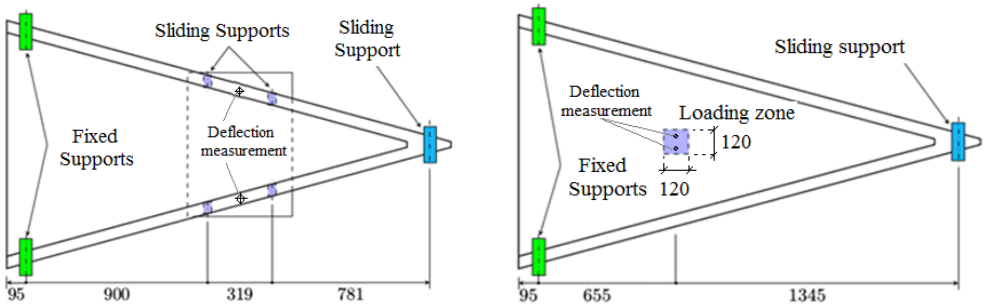

Figure 2. Loading configurations: 4 point bending tests (left side) ; centred bending tests (right side)

2.2. Experimental results

Figure 3 shows the experimental load-deflection curves for 4PBT and centred bending tests, respectively. The result of the specimen 2%-A-4pts-02 is not considered due to problems during casting inducing unexpected fiber distribution. Considering centred bending configuration, in order to take into account the influence of deviation in upper deck thickness among specimens

on the real stress field during loading, the curves displayed in Figure 3 show the applied force divided by the squared deck thickness as a function of the deflection. Detailed quantitative results can be found in (Guénet *et al.*, 2016).

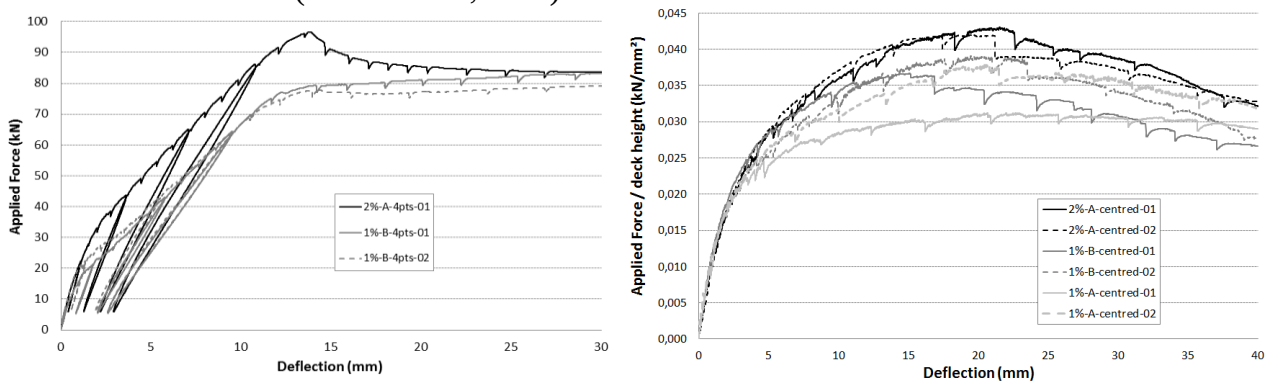

Figure 3. "Load-deflection" curves for 4PBT (at left) and "Load/h² - deflection" curves for centred bending tests (at right)

3. FEM Modeling

3.1. New damage micromechanics / rotating crack model

Considering a Representative Element Volume (REV) of the material, we identify two systems of loads: the external loads and the fibre bridging forces which have opposite directions. According to Linear Elastic Fracture Mechanics (LEFM), the resulting stress intensity factor is the difference between the stress intensity factors of each load. Considering the Irwin relationship ($G = K^2 / E$), the energy release rate can be formulated as proposed by (Bažant and Planas, 1998) as follows:

$$f = G_A + G_B - 2\sqrt{G_A G_B} - G_c \quad (1)$$

G_A is the energy release rate of the external loads: it is defined as the derivative of the free energy Ψ, by damage parameter $e \equiv N_c\, a^3$, assuming a penny-cracked shape of radius a and the Mori-Tanaka homogenization scheme (Dormieux *et al.*, 2006) which takes into account micro-cracks interaction (N_c is the number of cracks per mm^3). The resulting stiffness tensor is transverse-isotropic as the micromechanics model proposed by (Dormieux *et al.*, 2006). In our model we focus on the mode I fracture type by considering only one family of parallel cracks.

G_B is the energy release rate which takes into account the contribution of fibres as defined in (Li *et al.*, 1991):

$$G_B = N_c \frac{da}{de}\frac{\partial W_B(a)}{\partial a}, \text{ with } W_B(a) = 2\pi \int_0^a \int_0^w \sigma_c(w)\, r\, dw\, dr\ ,\ w \le L_f/2\ \text{, where} \quad (2)$$

W_B is the energy dissipated by fibres when forming a penny-shaped crack of radius a:

$$W_B(a) = 2\pi \int_0^a \int_0^w \sigma_c(w)\, r\, dw\, dr, \text{ with } w \le L_f/2\ \text{, where} \quad (3)$$

σ_c is the composite fibre stress proposed by (Lin and Li, 1997), as described in Sec. 3.3 ; it is first integrated according to crack opening before being integrated over the crack.
G_c is the fracture energy of the matrix G_f with N_c number of cracks per mm^3, written as a function of damage parameter.
The loading function Eq. (1) fulfils the Kuhn-Tucker condition:

$$f(e) < 0\ ;\ f(e)de = 0\ ;\ de \ge 0 \quad (4)$$

By solving system of Eq. (4) for a given strain history along with the consistency condition $df = 0$, the stress-strain material law of the material beyond the elastic part is derived.
This damage micromechanics approach is used to model the UHPFRC pseudo-strain hardening behavior. The hardening phase is over when the maximum composite fibre stress $\sigma_{c,max}$ is reached. The stress-strain material law is then derived from a smeared rotating crack model, smeared over a band of width L_0. The model continuity is ensured by a same approach to determine the fibre contribution based on (Li et al., 1991 ; Lin and Li, 1997) works.

3.2. Probability Distribution of fibres orientation

The fibre orientation distribution is described by Azimuth/Elevation coordinates and is taken as a bivariate normal-like probability density function $p_{\mu,\Sigma}(x)$ as follows (Tong, 1990):

$$p_{\mu,\Sigma}(x) = \frac{1}{2\pi\sqrt{|\Sigma|}} \exp\left[-\frac{1}{2}(x-\mu)^t \Sigma^{-1}(x-\mu)\right], \text{ where:} \quad (5)$$

$x = \langle E_l, A_z \rangle$ is the vector of random variables E_l and A_z, μ is the column-vector representing the function center and Σ is the covariance matrix (ζ is the rotation angle):

$$\mu = \begin{pmatrix} \mu_{A_z} \\ \mu_{E_l} \end{pmatrix} \quad (6)$$

$$\Sigma = \begin{pmatrix} (\sigma_{A_z}\cos\zeta)^2 + (\sigma_{E_l}\sin\zeta)^2 & ({\sigma_{A_z}}^2 - {\sigma_{E_l}}^2)\sin\zeta\cos\zeta \\ ({\sigma_{A_z}}^2 - {\sigma_{E_l}}^2)\sin\zeta\cos\zeta & (\sigma_{A_z}\sin\zeta)^2 + (\sigma_{E_l}\cos\zeta)^2 \end{pmatrix} \quad (7)$$

$$\alpha_{III} = \int_{A_z=0}^{2\pi} \int_{E_l=0}^{\frac{\pi}{2}} p_{\mu,\Sigma}(E_l, A_z) \cos^2 E_l \cos A_z \, dE_l \, dA_z \quad (8)$$

Figure 4 shows the evolution of fibre orientation factor α_i following parameters μ_{E_l} and σ_{E_l}.

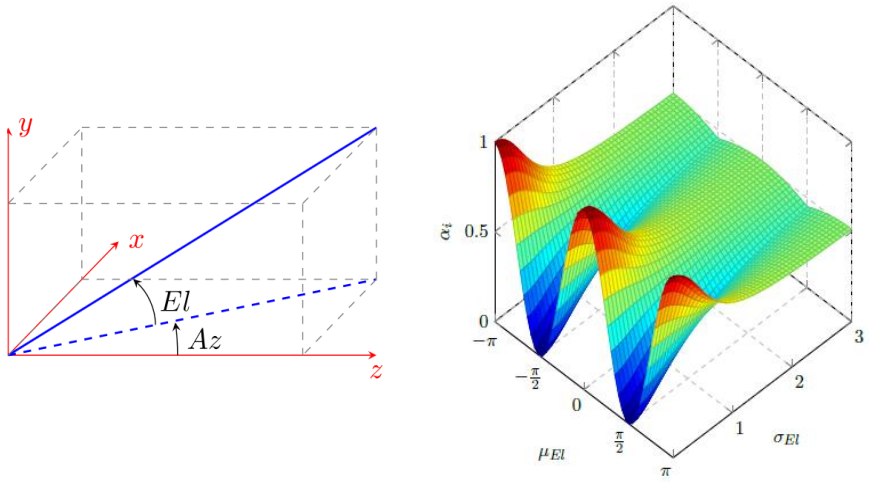

Figure 4. Evolution of fibre orientation factor following μ_{E_l} and σ_{E_l} (with $\mu_{E_l} = \mu_{A_z}$; $\sigma_{E_l} = \sigma_{A_z}$)

3.3. Extraction of fibres

The composite fibre stress σ_c is derived from the integration over the REV of the fibre pullout force $F(w)$ (Leung and Li, 1991) multiplied by the probability that the fibre intercepts the crack plane as proposed by (Lin and Li, 1997).

$$\sigma_c(w) = \frac{4v_f}{\pi\phi_f^2}\int_{A_z=0}^{2\pi}\int_{E_l=0}^{\frac{\pi}{2}}\int_{z=0}^{z_0\cos E_l\cos A_z} F(w)p(z,E_l,A_z)\cos E_l dz dE_l dA_z \quad \text{, where:} \qquad (9)$$

$$F(w) = \frac{1}{2}\phi_f\pi\sqrt{(1+\chi)\tau_0 E_f\phi_f w},\ w \le w_0 \text{ and } F(w) = \pi\phi_f\tau_0\frac{1+\chi}{L-w+w_0},\ w > w_0 \qquad (10)$$

$$\chi = \frac{E_f v_f}{E_m(1-v_f)} \text{ and } w_0 = \frac{4(1+\chi)\tau_0 L^2}{E_f\phi_f} \qquad (11)$$

z is the distance of centroid of fibre from crack plan and *p(z)* its probability distribution ; $p(z) = 2/L_f$ is chosen uniformly distributed in the REV. E_f: fibre module of elasticity ; E_m: matrix module of elasticity ; v_f: volume of fibres; *L*: embedded length of fibre; τ_0: bond strength of fibre-matrix interface and w_0 is the crack opening displacement at which the fibre is fully debonded.

4. Modeling the flexural tests of ribbed triangular plates

The model has been implemented in the open source Code_Aster finite element code.

4.1. Material model calibration

Prisms have been sawn out at different angles in the upper deck of additional triangular plates which have been cast with the same process as other specimens. From consideration of the casting process and loading configuration, two zones have been chosen to identify the fibres orientation: the "triangular base zone" and the "triangular top zone". For both zones, four inclinations have been studied (0°, 45°, 90° and 135°) from two additional specimens for each configuration (except for 1%-A-centred where only one additional triangular plate had been cast, so only one zone is considered). For each inclination, six prisms 60mm×35mm×240mm have been extracted and tested in four point bending configuration (total span equal to 210 mm and distance between upper rollers equal to 70 mm).

The model has been calibrated on the "stress-strain" or "stress-crack opening" relationships obtained from inverse analysis in considering the four inclinations for a given zone (NF P18-470, 2016). Table 3 is a list of calibrated values for each configuration (f_t = 8 MPa). Values of σ_{Az} > 50 is equivalent to considering an isotropic orientation of fiber in the extracted zone. For ribs of triangular plates, the model has been calibrated on the results of 4PBT on 70mm×70mm×280mm moulded prisms. Indeed fibres orientation inside 70mm×70mm×280mm molded prism is assumed to be similar to fibres orientation inside ribs (width equal to 60 mm) of triangular plates.

Table 3. Model parameters for each zone and each configuration

	τ_0(MPa)	L_0(mm)	N_c (/mm^3)	E_m (GPa)	μ_{E_l} (°)	μ_{A_z} (°)	σ_{E_l}	σ_{A_z}
1%-A-base-zone	15.05	0.72	-	50	0,0	34,9	0,160	0,480
1%-A-top-zone						3,3		0,228
1%-B-base-zone		1.00				48,5		49,27
1%-B-top-zone		0.59				isotropic		isotropic
2%-A-base-zone	10.95	1.34	1,48e^{-3}			-49,2	0,192	0,346
2%-A-top-zone		1.37				2,9		1,022

4.2. Four point flexural tests on triangular plates

The mesh used to reproduce experimental results is composed of tetrahedrons elements with linear interpolation functions for a total of 18,593 nodes. The nodes are equally dispatched. The

two reinforcing bars are modelled by 1D linear isotropic strain hardening bar elements with von Mises yield criterion. The comparison between the simulated and experimental load vs. deflection curves is shown in Figure 5 (left). In spite of the hypothesis of perfect bonding between UHPFRC and steel reinforcement, the model reasonably matches the experimental results.

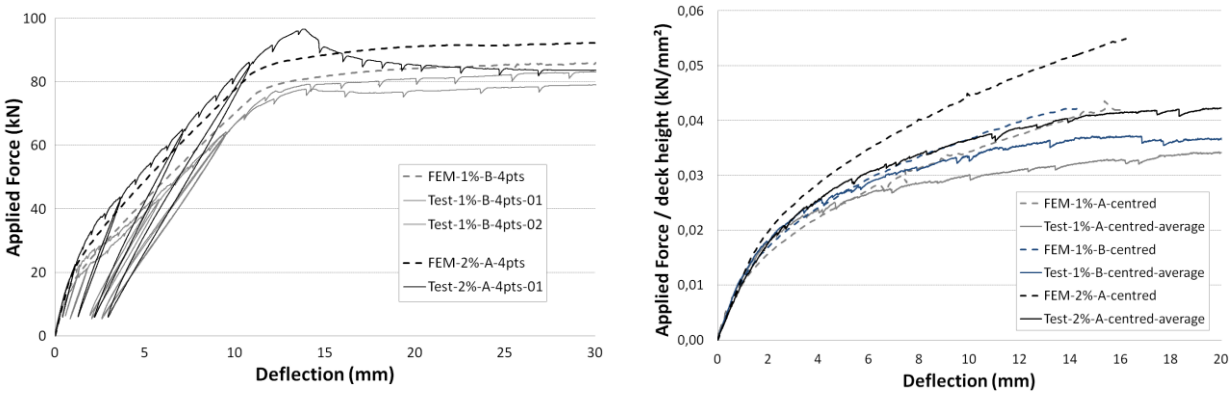

Figure 5. Comparison between experimental results and numerical modelling: 4PBTs (left) and centred bending tests (right)

4.3. Centred flexural tests on triangular plates

The mesh used to reproduce experimental results is composed of tetrahedron elements with linear interpolation functions for a total of 55,584 equally dispatched nodes. The mesh also takes advantage of the symmetric vertical plan. This simplification does not impact results because the principal tensile directions are in all zones transversal to fibres orientation (see Table 3). The comparison of the preliminary numerical simulation and the experimental results is presented in Figure 5 (right) and Figure 6. The damage location is correctly assessed. However, the numerical model overestimates the strength and stiffness of specimens during loading. The difference can be explained by the simplified boundary conditions which do not precisely model experimental observations (e.g., rotation of ribs and frictional contact). The overestimation of maximum bending strength in absence of non-linearity in compression may be also the reason. Finally, the use of linear elements instead of quadratics (torsion of ribs, shear interpolation) to reduce the CPU time in those preliminary calculation could also explain some differences.

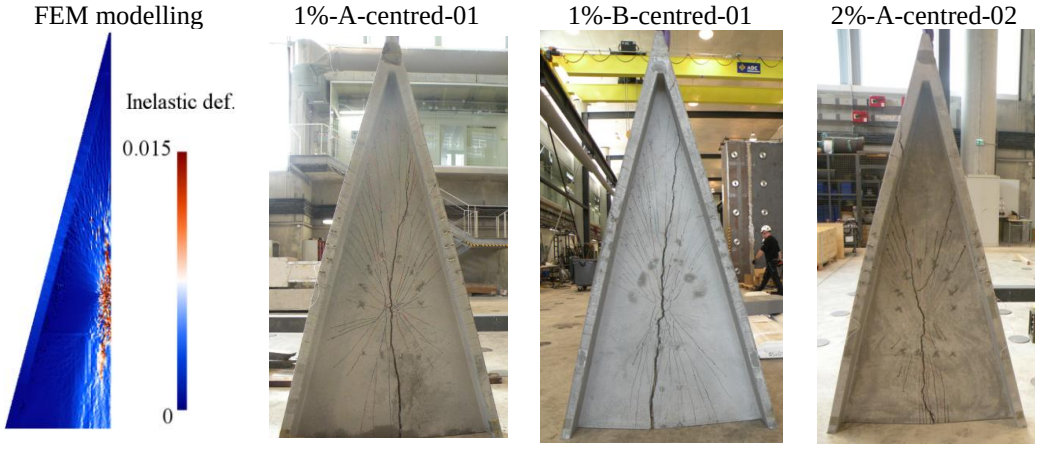

Figure 6. Examples of crack patterns for centred bending tests: experimental and numerical results

5. Conclusions

Flexural tests have been carried out in four point bending and centred bending configurations on ten reinforced ribbed triangular UHPFRC plates with different parameters such as fibres ratio (V_f =1% and 2%) or casting process. In order to identify the local UHPFRC post-cracking behavior in the structure, prisms have been cut in the upper deck, at different inclinations to determine the local fibre orientation. A new fracture-micromechanics/rotating crack model has been applied, taking into account the effect of fibre orientation in different zones of the tested ribbed triangular plates. Based on the encouraging preliminary analysis, the considered FEM tool allows predicting the maximum load, the failure mode and the crack pattern (Guénet *et al.*, 2016). Further studies are needed to capture more accurately the structural behaviour of such ribbed triangular plates.

6. References

NF P18-470, "Ultra High Performance Fiber Reinforced Concrete. Specification, performance, production and conformity", AFNOR (in French), 2016.

Bažant, Z. and Planas, J., "Fracture and size effect in concrete and other quasibrittle materials", New direction in civil engineering, CRC Press, 1998.

Dormieux, L., Kondo, D. and Ulm, F.J., "Microporomechanics", Wiley, 2006.

Guénet, T., Sorelli, L., Corvez, D., Bastien, J., Toutlemonde, F., Ferrier, E., Michel, L., "Analysis of a UHPFRC footbridge with a deck slab under bending by a novel fracture-micromechanics FEM model", UHPFRC 2013, RILEM PRO 87, 2013, pp. 519-528.

Guénet, T., Baby, F., Marchand, P., Sorelli, L., Bernardi, S., Toutlemonde, F., "Flexural failure modes and ductility assessment of ribbed triangular UHPFRC plates", Proceedings of Hipermat 2016 - 4th International Symposium on Ultra-High Performance Concrete and High Performance Construction Materials , March, Kassel, Germany.

Leung, C.K.Y. and Li, V.C., "New strength-based model for the debonding of discontinuous fibres in an elastic matrix", Journal of Material Science, Vol. 26, 1991, pp. 5996-6010.

Li, V.C., Wang, Y., and Backer, S., "A micromechanical model of tension-softening and bridging toughening of short random fiber reinforced brittle matrix composites", Journal of the Mechanics and Physics of Solids, Vol. 39 (5), 1991, pp. 607-625.

Lin, Z. and Li, V.C., "Crack bridging in fiber reinforced cementitious composites with slip hardening interfaces", J. Mech. Phys. Solids (UK), Vol. 45 (5), 1997, pp. 763-787.

Mazzacane, P., Ricciotti, R., Lamoureux, G., Corvez, D., "Roofing of the stade Jean Bouin in UHPFRC", UHPFRC 2013, RILEM PRO 87, 2013, pp. 59-68.

Ricciotti, R., Ricciotti, R., Mazzacane, P., "The Enrico Navarra Gallery", Designing and Building with UHPFRC", Toutlemonde & Resplendino eds, ISTE, 2011, pp. 79-86.

Sorelli, L., Ulm, F.J. and Toutlemonde, F., "Fracture stability and micromechanics of strain hardening cementitious composites", 6th Int. Conf. FRAMCOS, Catania, 2007, pp.1403-1411.

Tong, Y., "The Multivariate Normal Distribution", Springer, New York, 1990.

7. Acknowledgements

D. Corvez and †G. Chanvillard from LafargeHolcim are gratefully acknowledged for fruitful discussion and financial support to this program.